Analysis of rapidity spectra of negative pions in $d + {}^{12}C$, ${}^{12}C + {}^{12}C$, and ${}^{12}C + {}^{181}Ta$ collisions at 4.2 GeV/c per nucleon

Kh. K. Olimov,[1,2,*] Akhtar Iqbal,[1] V. V. Glagolev,[3] and Mahnaz Q. Haseeb[1,†]

[1]*Department of Physics, COMSATS Institute of Information Technology, Park Road, Islamabad, Pakistan*

[2]*Physical-Technical Institute of SPA "Physics-Sun" of Uzbek Academy of Sciences, Bodomzor Yo'li Street 2[b], 100084 Tashkent, Uzbekistan*

[3]*Joint Institute for Nuclear Research, RU-141980 Dubna, Russia*

(Received 11 October 2013; published 4 December 2013)

The experimental rapidity distributions of negative pions were studied in minimum bias $d + {}^{12}C$, ${}^{12}C + {}^{12}C$, and ${}^{12}C + {}^{181}Ta$ collisions at 4.2 GeV/c per nucleon with 4π acceptance. The quantitative analysis of centrality dependence of the rapidity as well as transverse momentum versus rapidity spectra of the negative pions in the above collisions was performed by fitting the pion spectra with a Gaussian function. The widths of the rapidity spectra of π^- mesons decreased in going from peripheral to central $d + {}^{12}C$, ${}^{12}C + {}^{12}C$, and ${}^{12}C + {}^{181}Ta$ collisions. With an increase in collision centrality, the centers of the rapidity distributions of the negative pions shifted towards the target fragmentation region in the case of asymmetric $d + {}^{12}C$ and ${}^{12}C + {}^{181}Ta$ collisions and remained at the midrapidity position for symmetric ${}^{12}C + {}^{12}C$ collisions. The extracted widths and locations of the centers of transverse momentum versus rapidity spectra of the negative pions did not depend within uncertainties on the masses of the projectile and target nuclei as well as the collision centrality. The experimental results were compared systematically with the corresponding results extracted by using a version of the quark-gluon-string model adapted to intermediate energies.

DOI: 10.1103/PhysRevC.88.064903 PACS number(s): 14.40.Be, 25.10.+s, 25.70.Mn

I. INTRODUCTION

Pions are abundantly produced in relativistic nuclear collisions and may, therefore, carry important information on collision dynamics. The negative pions can unambiguously be separated from the other products of nuclear collisions. The pions are particles produced dominantly at the energies of the Dubna synchrophasotron. The production of such particles in hadron-nucleus and nucleus-nucleus collisions at the energies of the order of a few GeV/nucleon is, to a large extent, due to the excitation of baryon resonances, which finally decay into nucleons and pions. It was shown in Refs. [1–9] that a significant fraction of the pions produced in relativistic hadron-nucleus and nucleus-nucleus collisions in bubble chamber experiments of the Joint Institute for Nuclear Research (JINR, Dubna, Russia) originated from decay of Δ resonances. The dominant role of Δ resonances in pion production at the energies of the order of a few GeV/nucleon or less was also revealed in earlier papers [10–14]. The decay kinematics of Δ resonances was shown to be responsible for low transverse momentum enhancement of pion spectra in hadron-nucleus and nucleus-nucleus collisions at incident beam energies from 1 to 15 GeV per nucleon [9,13,14]. It was observed that the pions that come from Δ decay mainly populated the low transverse momentum part of the spectrum [9,13,14].

The energy as well as the transverse momentum spectra of the pions exhibit two slope shapes that correspond to two different temperatures as shown earlier in Refs. [10,15–19]. In Ref. [15], the two-temperature shape of the center-of-mass (c.m.) kinetic-energy spectra of the negative pions in Ar + KCl at 1.8 GeV/nucleon was obtained. In this paper, the occurrence of two temperatures T_1 and T_2 was interpreted as due to two channels of pion production: pions that come from Δ resonance decay (T_1) and directly produced pions (T_2). In Ref. [10], the two-temperature shape of the kinetic-energy spectrum of pions emitted at 90° in the center-of-mass system (c.m.s.) of central La + La collisions at 1.35 GeV/nucleon was interpreted as due to different contributions of Δ's that originate from the early and later stages of heavy-ion reactions. The two-temperature behavior also was observed for c.m. energy as well as p_t spectra of π^- mesons produced in Mg + Mg collisions [16] at the incident momentum of 4.2–4.3A GeV/c. In Ref. [17], the two-temperature shape of the experimental c.m. energy spectra of π^- in ${}^{12}C + {}^{12}C$ collisions at 4.2A GeV/c was explained by the superposition of partial contributions from different sources (decays of resonances, direct reactions, etc.) by analyzing the spectra of π^- that come from different sources in the framework of the quark-gluon-string model (QGSM).

In our recent papers [18,19], the spectral temperatures of π^- mesons in $d + {}^{12}C$, ${}^{4}He + {}^{12}C$, and ${}^{12}C + {}^{12}C$ collisions at 4.2A GeV/c were extracted by fitting the transverse momentum spectra of π^- by the one-temperature and two-temperature Hagedorn functions as given by the Hagedorn-Rafelski [20] and the Hagedorn-Ranft [21] thermodynamic models. The average spectral temperatures of the negative pions were extracted from the p_t and scaled c.m. kinetic-energy spectra of π^- in ${}^{12}C + {}^{12}C$ collisions at 4.2A GeV/c for different intervals of c.m. rapidity and c.m. emission angle of π^- [19] by using fits with the one-temperature Hagedorn and one-temperature Boltzmann distribution functions, respectively. It was shown that the experimental p_t spectra of π^- were fitted

*olimov@comsats.edu.pk

†mahnazhaseeb@comsats.edu.pk

significantly better by the Hagedorn function with two temperatures T_1 and T_2 as compared to the one-temperature fit. The major contribution ($R_1 \sim 90\%$) to the total multiplicity of the π^- mesons came from spectral temperature $T_1 \sim 78$–84 MeV, whereas, the relative yield of the high-temperature $T_2 \sim 146$–155-MeV component was much lower ($R_2 \sim 10\%$) [18]. The spectral temperatures T_1 and T_2 and their relative contributions did not depend, within fitting errors, on the degree of collision centrality in ^{12}C + ^{12}C collisions at 4.2A GeV/c. The spectral temperatures of the π^- mesons extracted in Ref. [18] from the transverse momentum spectra were noticeably lower than those of the negative pions in d + ^{12}C, ^{4}He + ^{12}C, and ^{12}C + ^{12}C collisions at 4.2A GeV/c deduced in an early paper [17] from the analysis of the noninvariant c.m. energy spectra of π^-. It was concluded [18] that p_t spectra of π^- were preferable for the adequate estimation of the spectral temperatures of π^- as compared to the scaled c.m. kinetic-energy spectra due to the Lorentz invariance of the p_t spectra with respect to longitudinal boosts.

Information about the state of excited or/and compressed nuclear matter created in relativistic nucleus-nucleus collisions, collision dynamics, and the particle production mechanism could be extracted from the analysis of the collision centrality dependence of the rapidity and transverse momentum spectra of pions [10,22–25]. The momentum, transverse momentum, and rapidity distributions of negative pions produced in Mg + Mg collisions at 4.3 GeV/c per nucleon were analyzed in Ref. [25]. Analysis of pion rapidity distribution showed that the central rapidity region was occupied with pions of significantly larger transverse momentum as compared to the fragmentation region of interacting nuclei [25]. The experimental results were compared with the QGSM. The rapidity distributions of the negative pions in (p,d,α,C) + C and (d,α,C) + Ta collisions at 4.2A GeV/c were analyzed in different transverse momentum intervals of π^- mesons in Refs. [23,24]. With an increase in the transverse momentum of the π^- mesons, the fraction of negative pions in the central rapidity region increased, and the corresponding fraction in the fragmentation region of colliding nuclei decreased. Negative pions with large transverse momentum were mainly concentrated in the central rapidity interval [23,24]. The centrality dependence of the pion rapidity spectra in minimum bias ^{12}C + ^{12}C and ^{12}C + ^{181}Ta collisions at a momentum of 4.2 GeV/c per nucleon was partly studied in Ref. [22] on statistics of 7900 ^{12}C + ^{12}C and 2000 ^{12}C + ^{181}Ta inelastic collision events, which is less than half the total statistics of inelastic ^{12}C + ^{12}C and ^{12}C + ^{181}Ta collision events used in the present analysis. It was observed [22] that the pion rapidity spectrum resembled a Gaussian shape regardless of the target mass number and collision centrality and that the QGSM could reproduce the main features of pion rapidity as well as transverse momentum spectra quite well [22].

The present analysis is a continuation of our recent papers [18,19] devoted to the analysis of various characteristics of negative pions produced in nucleus-nucleus collisions at 4.2 GeV/c per nucleon. We aim to study the dependences of experimental rapidity distributions of negative pions, produced in d + ^{12}C,^{12}C + ^{12}C, and ^{12}C + ^{181}Ta collisions at a momentum of 4.2 GeV/c per nucleon, as well as the dependences of the average transverse momenta of negative pions on their rapidity, the mass numbers of projectile and target nuclei, and degree of collision centrality. All the experimental results will systematically be compared with the corresponding results extracted by using the QGSM [26–29]. This analysis will enable the extraction of interesting information on the extent of change in the shape of the rapidity spectra of the produced negative pions and its dependences on the masses of projectile and target nuclei as well as the collision centrality. To see the influence of nuclear effects, if any, on rapidity as well as the transverse momentum versus rapidity spectra of the negative pions, the spectra of π^- mesons in d + ^{12}C,^{12}C + ^{12}C, and ^{12}C + ^{181}Ta collisions at 4.2A GeV/c will be compared with the corresponding spectra of π^- in proton-proton collisions at the same incident momentum per nucleon. The results that come from the present analysis may be useful to help interpret the relevant experimental data obtained from high-energy heavy-ion collisions. The paper is organized as follows. The quark-gluon-string model is briefly described in Sec. II. The experimental procedures are presented in Sec. III. The analysis of negative pion rapidity spectra is given in Sec. IV. Section V contains the summary and conclusions of the present paper.

II. THE QGSM

The QGSM was developed to describe hadron-nucleus and nucleus-nucleus collisions at high energies [26–29]. In the QGSM, hadron production takes place via the formation and decay of quark-gluon strings. This model is used as a basic process for the generation of hadron-hadron collisions. In the present analysis, we used the version of the QGSM [27] adapted to the range of intermediate energies ($\sqrt{s_{nn}} \leqslant 4$ GeV). The incident momentum of 4.2 GeV/c per nucleon for the collisions analyzed in the present paper corresponds to incident kinetic energy 3.37 GeV per nucleon and nucleon-nucleon c.m.s. energy $\sqrt{s_{nn}} = 3.14$ GeV. The QGSM is based on Regge and string phenomenologies of particle production in inelastic binary hadron collisions. To describe the evolution of the hadron and quark-gluon phases, a coupled system of Boltzmann-like kinetic equations was used in the model. The nuclear collisions were treated as a superposition of independent interactions of the projectile and target nucleons, stable hadrons, and short-lived resonances. Resonant reactions, such as $\pi + N \to \Delta$, pion absorption by NN quasideuteron pairs, and $\pi + \pi \to \rho$ were taken into account in this model. The time of the formation of hadrons also was included in the QGSM. The masses of strings at intermediate energies are very small. At c.m.s. energy $\sqrt{s_{nn}} = 3.14$ GeV, the masses of the strings are smaller than 2 GeV, and these strings fragment predominantly (∼90%) through a two-particle decay channel.

The nucleon coordinates in the colliding nuclei were generated according to the realistic nuclear matter density. The sphere of the nucleus was filled with the nucleons subject to the condition that the distance between nucleons was greater than 0.8 fm. The Fermi motion of the nucleons inside the nucleus was taken into account in the model. The nucleon momenta p_N were distributed in the range of $0 \leqslant p_N \leqslant p_F$, where p_F is the maximum Fermi momentum

of a nucleon for a given nucleus, determined by its nuclear density. The procedure of the generation of a collision event in the QGSM consisted of three steps: (i) defining the configurations of the colliding nucleons, (ii) production of quark-gluon strings, and (iii) the breakup (fragmentation) of strings into observed hadrons. For simulating the nucleon-nucleon and pion-nucleon interactions in the QGSM, the binary, "undeveloped" cylindrical, diffractive, cylindrical, and planar topological quark diagrams were used [21–24]. The binary processes give the main contribution to the QGSM and correspond to a quark rearrangement (in an interacting pair of nucleons) without direct particle emission in the string decay. This process mainly results in resonance production (for example, in reactions $p + n \rightarrow p + \Delta^0$, $p + p \rightarrow n + \Delta^{++}$, $n + n \rightarrow p + \Delta^-$, $n + n \rightarrow n + \Delta^0$, etc.), and the resonances are the main source of pion production in the QGSM.

The transverse momenta of pions produced in quark-gluon string fragmentation processes are the product of two factors: (i) string motion on the whole as a result of the transverse motion of the constituent quarks and (ii) $q\bar{q}$ pair production from the breakup of the string. The transverse motion of quarks inside hadrons was described by the Gaussian distribution with variance $\sigma^2 \cong 0.3$ (GeV/c)^2. The transverse momentum k_T of produced $q\bar{q}$ quark pairs in the c.m.s. of the string was defined according to a distribution $W(k_T) = \frac{3b}{\pi(1+bk_T^2)^4}$, where $b = 0.34$ (GeV/c)$^{-2}$. For hadron interactions, the cross sections were taken from the experimental data. Isotopic invariance and predictions of the additive quark model (for meson-meson cross sections, etc.) were used to avoid data deficiency. The resonance interaction cross sections were taken to be equal to the interaction cross sections of the stable particles with the same quark content. The decay of the excited recoil nuclear fragments and a coupling of nucleons inside the nucleus were not taken into account in the QGSM.

III. THE EXPERIMENT

The data analyzed in the present paper were obtained by using the 2-m propane (C_3H_8) bubble chamber of the Laboratory of High Energies of JINR (Dubna, Russia). The 2-m propane bubble chamber was placed in a magnetic field of strength 1.5 T [22,30–36]. Three tantalum ^{181}Ta foils also were placed in the experimental setup of the chamber. The thickness of each foil was 1 mm, and the separation distance between foils was 93 mm. The bubble chamber then was irradiated with beams of ^{2}H and ^{12}C nuclei accelerated to a momentum of 4.2 GeV/c per nucleon at the Dubna synchrophasotron. The deuterons and ^{12}C nuclei were made to interact with the carbon nuclei and protons of the propane molecules and the tantalum ^{181}Ta foils placed in the propane bubble chamber [22,34–36]. Methods of selection of inelastic $d + {}^{12}$C, ^{12}C + ^{12}C, and ^{12}C + ^{181}Ta collision events in this experiment were explained in detail in Refs. [22,34–36]. The threshold for the detection of the negative pions in the propane bubble chamber was 70 MeV/c for $d + {}^{12}$C and ^{12}C + ^{12}C collisions, whereas, for ^{12}C + ^{181}Ta collisions, it was 80 MeV/c. In some momentum and angular intervals, the particles could not be detected with 100% efficiency. To account for small losses of particles emitted under large angles to the object plane of the camera and due to tantalum foils, the relevant corrections were introduced as discussed in Refs. [22,34–36]. The average uncertainty in the measurement of the emission angle of the negative pions was 0.8°. The mean-relative uncertainty of the momentum measurement of the π^- mesons from the curvature of their tracks in the propane bubble chamber was 6%. All the negative particles, except identified electrons, were considered to be π^- mesons. Admixtures of the unidentified electrons and the negative strange particles among them were less than 5% and 1%, respectively. In our experiment, the spectator protons are protons with momenta $p > 3$ GeV/c and emission angle $\theta < 4°$ (projectile spectators) and protons with momenta $p < 0.3$ GeV/c (target spectators) [22,34–36]. Hence, the participant protons are those protons which remain after the elimination of the spectator protons.

The statistics of the experimental data analyzed in the present paper consist of 7071, 20 528, and 2420 $d + {}^{12}$C, ^{12}C + ^{12}C, and ^{12}C + ^{181}Ta minimum bias inelastic collision events, respectively, with practically all the secondary charged particles detected with 4π acceptance. For systematic comparison with the experimental data, we simulated 30 000 minimum bias inelastic collision events for each $d + {}^{12}$C and ^{12}C + ^{12}C collision system at 4.2 GeV/c per nucleon and 6000 ^{12}C + ^{181}Ta minimum bias inelastic collision events at 4.2A GeV/c by using the quark-gluon-string model adapted to intermediate energies. To simulate the real experimental conditions, the QGSM events were passed through a "filter." As a result of this filtering procedure, all the slow particles absorbed in the 2-mm propane layer and in tantalum foils were excluded.

Comparison of the mean multiplicities per event of the negative pions and participant protons and the average values of rapidity and the transverse momentum of the π^- mesons in $d + {}^{12}$C, ^{12}C + ^{12}C and ^{12}C + ^{181}Ta collisions at 4.2 GeV/c per nucleon both in the experiment and in the QGSM is presented in Table I.

IV. ANALYSIS OF PION RAPIDITY SPECTRA

Comparison of the experimental and QGSM rapidity distributions of the negative pions in $d + {}^{12}$C, ^{12}C + ^{12}C, and ^{12}C + ^{181}Ta collisions at a momentum of 4.2 GeV/c per nucleon is shown in Fig. 1(a). All the spectra in Fig. 1 and the figures that follow are plotted in the c.m.s. of nucleon-nucleon collisions at 4.2 GeV/c (the rapidity of the center of mass of a nucleon-nucleon collision is $y_{\text{c.m.s.}} \approx 1.1$ at this incident momentum). Rapidity distribution of the negative pions in ^{12}C + ^{12}C collisions is symmetric with respect to midrapidity $y_{\text{c.m.}} = 0$ as expected for a system with identical projectile and target nuclei. It can be seen from Fig. 1(a) that, with increases in both the projectile and the target nuclei masses, the height of rapidity distributions (hence, the multiplicity of π^- mesons) increases. Rapidity distribution of π^- shifts towards lower rapidities as observed from Fig. 1(a) or more towards the target fragmentation region as the mass of the target nucleus increases while going from ^{12}C + ^{12}C to ^{12}C + ^{181}Ta collisions. This is because the effective number of the target participant nucleons

TABLE I. Mean multiplicities per event of negative pions and participant protons and the average values of the rapidity and transverse momentum of π^- mesons in $d + {}^{12}$C, ^{12}C + ^{12}C, and ^{12}C + ^{181}Ta collisions at 4.2 GeV/c per nucleon. The mean rapidities are calculated in the c.m.s. of the nucleon-nucleon collisions at 4.2 GeV/c. Only statistical errors are given here and in the tables that follow.

Type		$\langle n(\pi^-)\rangle$	$\langle n_{\text{part.prot.}}\rangle$	$\langle y_{\text{c.m.}}(\pi^-)\rangle$	$\langle p_t(\pi^-)\rangle$(GeV/$c$)
$d + {}^{12}$C	Expt.	0.66 ± 0.01	1.95 ± 0.02	−0.12 ± 0.01	0.252 ± 0.003
	QGSM	0.64 ± 0.01	1.86 ± 0.01	−0.17 ± 0.01	0.222 ± 0.002
^{12}C + ^{12}C	Expt.	1.45 ± 0.01	4.35 ± 0.02	−0.016 ± 0.005	0.242 ± 0.001
	QGSM	1.59 ± 0.01	4.00 ± 0.02	0.007 ± 0.005	0.219 ± 0.001
^{12}C + ^{181}Ta	Expt.	3.50 ± 0.10	13.3 ± 0.2	−0.34 ± 0.01	0.217 ± 0.002
	QGSM	5.16 ± 0.09	14.4 ± 0.2	−0.38 ± 0.01	0.191 ± 0.001

and, hence, the number of π^- mesons produced in the target fragmentation region increase with an increase in the mass of the target nucleus. As seen from Fig. 1(a), the QGSM satisfactorily describes the experimental rapidity distributions of the π^- mesons in $d + {}^{12}$C, ^{12}C + ^{12}C, and ^{12}C + ^{181}Ta collisions. Figure 1(b) shows that the experimental rapidity spectra of the negative pions in the analyzed collisions can be fitted well by the Gaussian distribution function given by

$$F(y) = \frac{A_0}{\sigma}\exp\left(\frac{-(y-y_0)^2}{2\sigma^2}\right), \qquad (1)$$

where σ is the standard deviation, referred to as a width of distribution in the present work, y_0 is the center of the Gaussian distribution, and A_0 is the fitting constant. Parameters extracted from fitting the rapidity spectra of the negative pions in $d + {}^{12}$C, ^{12}C + ^{12}C, and ^{12}C + ^{181}Ta collisions at 4.2 GeV/c per nucleon with the Gaussian function in Eq. (1) are presented in Table II. As seen from Table II, the widths of the rapidity distributions of the π^- mesons practically coincided in $d + {}^{12}$C and ^{12}C + ^{12}C collisions, whereas, it was slightly lower in the case of ^{12}C + ^{181}Ta collisions both in the experiment and in the QGSM. The widths of the experimental

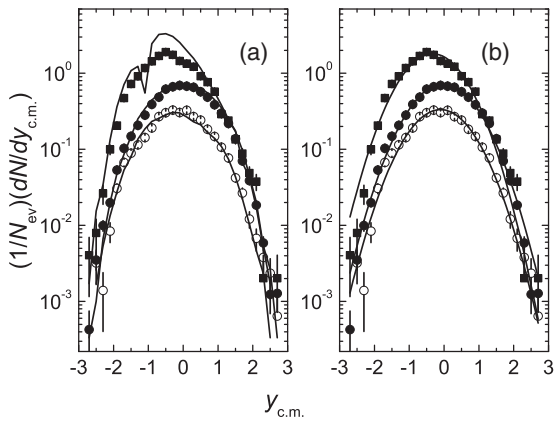

FIG. 1. The experimental rapidity distributions of the negative pions in $d + {}^{12}$C (○), ^{12}C + ^{12}C (●), and ^{12}C + ^{181}Ta (■) collisions at 4.2A GeV/c. The corresponding (a) QGSM spectra and (b) fits with the Gaussian function are given by the solid lines. All the spectra are obtained in the c.m.s. of the nucleon-nucleon collisions at 4.2 GeV/c. The distributions are normalized by the total number N_{ev} of the corresponding inelastic events.

rapidity spectra of the negative pions ($\sigma^{\text{C+C}} = 0.793 \pm 0.003$ and $\sigma^{\text{C+Ta}} = 0.75 \pm 0.01$), extracted in the present analysis, proved to be slightly smaller than the corresponding widths ($\sigma^{\text{C+C}} \approx 0.82$ and $\sigma^{\text{C+Ta}} \approx 0.79$) estimated in Ref. [22] for ^{12}C + ^{12}C and ^{12}C + ^{181}Ta collision events at 4.2 GeV/c on the total experimental statistics, which was less than half the corresponding statistics used in the present paper. It is evident from Table II that the locations of centers y_0, extracted from fitting the rapidity spectra of the π^- mesons with the Gaussian function, coincided within uncertainties with the corresponding mean rapidities of the negative pions in the analyzed collisions given in Table I. As follows from Table II, the QGSM satisfactorily describes the widths as well as the locations of y_0 of the rapidity distributions of the negative pions in $d + {}^{12}$C, ^{12}C + ^{12}C, and ^{12}C + ^{181}Ta collisions at 4.2 GeV/c per nucleon.

It is of interest to quantitatively analyze the change in shape of the rapidity spectra of the negative pions with an increase in the collision centrality, which corresponds to a decrease in the impact parameter of collision. Since the impact parameter is not directly measurable, we use the number of participant protons N_p to characterize the collision centrality. We follow Refs. [22,37] to define the peripheral collision events to be those in which $N_p \leqslant \langle n_{\text{part.prot.}}\rangle$ and the central collisions as the collision events with $N_p \geqslant 2\langle n_{\text{part.prot.}}\rangle$, where $\langle n_{\text{part.prot.}}\rangle$ is the mean multiplicity per event of the participant protons. It was shown in Ref. [37] that the central ^{12}C + ^{181}Ta collisions at 4.2A GeV/c, selected by using the above criterion, were characterized by complete projectile stopping because in these collisions the average number $\langle \nu^p \rangle$ of the interacting projectile nucleons was very close to the total number of nucleons in projectile carbon. Fractions of central and peripheral $d + {}^{12}$C, ^{12}C + ^{12}C, and ^{12}C + ^{181}Ta collision events, relative to the total inelastic cross section, obtained in the present paper for both experimental and QGSM data, are presented in Table III. As seen from Table III, the experimental and corresponding model fractions of the central and peripheral $d + {}^{12}$C, ^{12}C + ^{12}C, and ^{12}C + ^{181}Ta collision events coincide with each other within two standard errors with the only exception that the fraction of peripheral $d + {}^{12}$C collisions is overestimated by the QGSM. As seen from Table III, the central interactions constitute about 10% in $d + {}^{12}$C and ^{12}C + ^{12}C collisions, whereas, it is approximately 15% in ^{12}C + ^{181}Ta collisions. On the other hand, the fraction of peripheral collisions is roughly 60% in the analyzed collisions. These results for ^{12}C + ^{12}C

TABLE II. Parameters extracted from fitting the rapidity spectra of the negative pions in $d + {}^{12}$C, ^{12}C + ^{12}C, and ^{12}C + ^{181}Ta collisions at 4.2 GeV/c per nucleon with the Gaussian function; n.d.f. represents the number of degrees of freedom.

Type		A_0	σ	y_0	χ^2/n.d.f.	R^2 value
$d + {}^{12}$C	Expt.	0.260 ± 0.004	0.78 ± 0.01	−0.10 ± 0.01	2.88	0.983
	QGSM	0.250 ± 0.003	0.80 ± 0.01	−0.17 ± 0.01	5.13	0.986
^{12}C + ^{12}C	Expt.	0.575 ± 0.004	0.793 ± 0.003	−0.016 ± 0.005	8.93	0.992
	QGSM	0.624 ± 0.004	0.786 ± 0.003	0.009 ± 0.005	14.21	0.983
^{12}C + ^{181}Ta	Expt.	1.36 ± 0.02	0.75 ± 0.01	−0.33 ± 0.01	7.66	0.971
	QGSM	1.78 ± 0.02	0.71 ± 0.01	−0.30 ± 0.01	53.43	0.878

and ^{12}C + ^{181}Ta collisions coincide with the fractions of the central and peripheral collision events estimated in Ref. [22] on significantly lower statistics of ^{12}C + ^{12}C and ^{12}C + ^{181}Ta collisions as compared to the corresponding statistics of the present analysis.

In Figs. 2 and 3, the rapidity distributions of the negative pions are compared for central and peripheral $d + {}^{12}$C, ^{12}C + ^{12}C, and ^{12}C + ^{181}Ta collision events in the experiment and QGSM, respectively. All the spectra of Figs. 2 and 3 are fitted with the Gaussian function given in Eq. (1). The corresponding parameters extracted from fitting the experimental and QGSM spectra for the central and peripheral collisions are given in Table IV. In general, as can be seen from Figs. 2 and 3 and Table IV, all the spectra are fitted satisfactorily with the Gaussian function. As follows from Table IV, the widths of the experimental rapidity spectra of the negative pions decrease by $(8 \pm 2)\%$, $(5 \pm 1)\%$, and $(15 \pm 2)\%$ in going from peripheral to central $d + {}^{12}$C, ^{12}C + ^{12}C, and ^{12}C + ^{181}Ta collisions, respectively. A similar decrease in the estimated widths of the rapidity spectra of the negative pions was observed in Ref. [22] in going from peripheral to central ^{12}C + ^{12}C and ^{12}C + ^{181}Ta collisions at 4.2A GeV/c. The widths estimated for peripheral and central ^{12}C + ^{12}C and ^{12}C + ^{181}Ta collisions ($\sigma^{\mathrm{C+C}}_{\mathrm{periph}} \approx 0.85$ and $\sigma^{\mathrm{C+C}}_{\mathrm{centr}} \approx 0.78$, $\sigma^{\mathrm{C+Ta}}_{\mathrm{periph}} \approx 0.87$ and $\sigma^{\mathrm{C+Ta}}_{\mathrm{centr}} \approx 0.74$) in Ref. [22] proved to be slightly larger as compared to the corresponding widths of the experimental rapidity spectra shown in Table IV. The values of widths obtained in the present analysis agree with the results of Ref. [38] where the width of the pseudorapidity distribution for the shower particles changed from 0.74 for most central to 0.94 for most peripheral collisions. As can be seen from Figs. 2(a), 2(c), and Table IV, the centers y_0 of the rapidity distributions of the π^- mesons shift by -0.32 ± 0.04 and -0.44 ± 0.02 units towards the target fragmentation region while going from peripheral to central $d + {}^{12}$C and ^{12}C + ^{181}Ta collisions, respectively. In the case of the corresponding QGSM spectra, as seen from Figs. 3(a), 3(c), and Table IV, the centers y_0 of the rapidity distributions of the negative pions also shift by -0.22 ± 0.02 and -0.39 ± 0.02 units towards the target fragmentation region in $d + {}^{12}$C and ^{12}C + ^{181}Ta, collisions, respectively. Such shifts in centers y_0 of the rapidity spectra of the π^- mesons in $d + {}^{12}$C and ^{12}C + ^{181}Ta collisions are caused by an increase in the rescattering effects in the target nuclei, which are heavier than the projectile nuclei, and the subsequent increase in the number of the target participant nucleons (and, hence, the increase in the number of pions produced in the target fragmentation region) as the collision centrality increases. We observe a larger shift in the case of ^{12}C + ^{181}Ta collisions as compared to $d + {}^{12}$C collisions, which is likely due to the fact that $\frac{A({}^{181}\mathrm{Ta})}{A({}^{12}\mathrm{C})} > \frac{A({}^{12}\mathrm{C})}{A({}^{2}\mathrm{H})}$. As seen from Figs. 2(b), 3(b), and Table IV, we do not observe such a shift with increasing centrality in the case of the rapidity spectra of the negative pions in ^{12}C + ^{12}C collisions in the experiment as well as the QGSM. This is most likely due to the symmetry of the colliding ^{12}C + ^{12}C system in which the effective numbers of participant nucleons from target

TABLE III. Fractions of central and peripheral $d + {}^{12}$C, ^{12}C + ^{12}C, and ^{12}C + ^{181}Ta collisions at 4.2 GeV/c per nucleon relative to the total inelastic cross section.

Type	Central collisions (%)		Peripheral collisions (%)	
	Experiment	QGSM	Experiment	QGSM
$d + {}^{12}$C	10 ± 1	12 ± 1	53 ± 1	73 ± 1
^{12}C + ^{12}C	11 ± 1	8 ± 1	58 ± 1	62 ± 1
^{12}C + ^{181}Ta	16 ± 1	15 ± 1	60 ± 2	56 ± 1

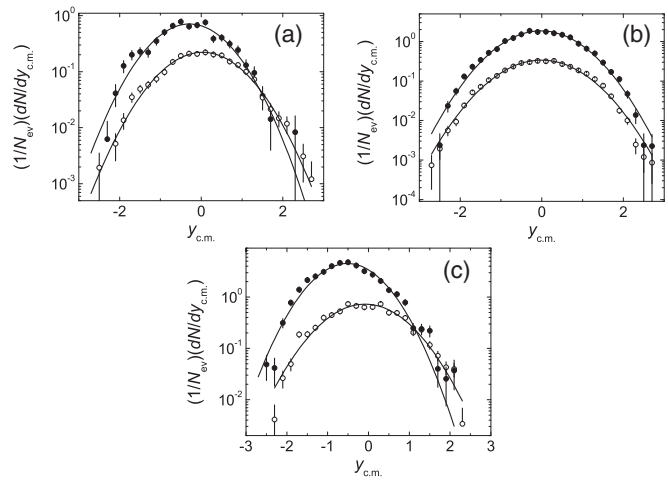

FIG. 2. The experimental rapidity distributions of the negative pions in the central (•) and peripheral (○) collision events in (a) d + ^{12}C, (b) ^{12}C + ^{12}C, and (c) ^{12}C + ^{181}Ta collisions at 4.2A GeV/c. The corresponding fits with the Gaussian function are given by the solid lines. All the spectra are obtained in the c.m.s. of the nucleon-nucleon collisions at 4.2 GeV/c.

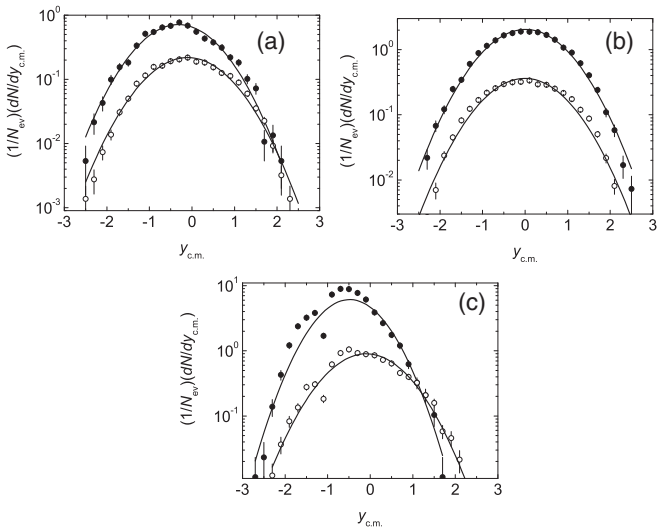

FIG. 3. Rapidity distributions of the negative pions calculated by using the QGSM in the central (•) and peripheral (○) collision events in (a) $d + {}^{12}$C, (b) ^{12}C + ^{12}C, and (c) ^{12}C + ^{181}Ta collisions at 4.2A GeV/c. The corresponding fits with the Gaussian function are given by the solid lines. All the spectra are obtained in the c.m.s. of the nucleon-nucleon collisions at 4.2 GeV/c.

and projectile ^{12}C nuclei (and, hence, the numbers of pions produced around target and projectile fragmentation regions) practically remain the same in both central and peripheral collisions. Therefore, the rapidity distribution of the negative pions in ^{12}C + ^{12}C collisions remains symmetric around $y_{\text{c.m.}} = 0$ with increasing collision centrality. As observed from Figs. 2, 3, and Table IV, the peaks and centers y_0 of the rapidity spectra of the π^- mesons in peripheral $d + {}^{12}$C and ^{12}C + ^{181}Ta collisions proved to be close to $y_{\text{c.m.}} = 0$. This can be due to the reason that, in the case of peripheral collisions, the effective volumes of the interacting regions in both the target and the projectile nuclei (and, thus, the corresponding numbers of the interacting nucleons) are close to each other.

It seems interesting to compare the widths of the rapidity spectra of the negative pions extracted in central nucleus-nucleus collisions at 4.2A GeV/c with the corresponding widths of the rapidity spectra of the negative pions and charged kaons produced in central Pb + Pb collisions at 20A and 30A GeV, extracted recently in Ref. [39] by the NA49 Collaboration by using the fit with the Gaussian function. The widths of the rapidity spectra of the negative pions and charged kaons in central Pb + Pb collisions at 20A and 30A GeV are presented in Table V. As seen from Tables IV and V, the widths of the rapidity spectra of the π^- mesons in central $d + {}^{12}$C, ^{12}C + ^{12}C, and ^{12}C + ^{181}Ta collisions at 4.2A GeV/c are noticeably smaller as compared to the corresponding widths of the negative pions in central Pb + Pb collisions at 20A and 30A GeV. This observation agrees with a weak increase in width for π^- as incident energy increases from 20A to 30A GeV, as seen from Table V. Due to the symmetry of the colliding systems, it seems appropriate to compare the widths extracted in central ^{12}C + ^{12}C collisions at 4.2A GeV/c with the corresponding widths obtained in central Pb + Pb collisions at 20A and 30A GeV. As observed from Tables IV and V, the width for π^- in central ^{12}C + ^{12}C collisions is slightly smaller than the corresponding widths for the negative pions in central Pb + Pb collisions, which, as stated above, agrees with a weak growth of the width with an increase in incident energy per nucleon. As seen from Table V, the widths of the rapidity spectra of K^+ and K^- mesons also increase in central Pb + Pb collisions with an increase in incident energy from 20A to 30A GeV. It should be noted that the widths for π^- in both central ^{12}C + ^{12}C and Pb + Pb collisions proved to be noticeably larger than the corresponding widths of the rapidity spectra of K^+ and K^- mesons in central Pb + Pb collisions. This is likely due to the significantly higher-energy threshold for the production of charged kaons as compared to that for pions. Hence, the K^+ and K^- mesons generally are produced at harder collisions with larger momentum transfers as compared to negative pions. Therefore, charged kaons are grouped and are located closer to and around center-of-mass rapidity on the rapidity axis as compared to the negative pions, which results in significantly smaller widths of the rapidity spectra of kaons than that for pions.

Here, the relevant results on the rapidity spectra of the participant protons in ^{12}C + ^{12}C and ^{12}C + ^{181}Ta collisions at 4.2 GeV/c per nucleon, analyzed in detail in Ref. [22], are

TABLE IV. Parameters obtained from fitting the rapidity spectra of the negative pions in central and peripheral $d + {}^{12}$C, ^{12}C + ^{12}C, and ^{12}C + ^{181}Ta collisions at 4.2 GeV/c per nucleon with the Gaussian function.

	Type	A_0	σ	y_0	χ^2/n.d.f.	R^2 value
$d + {}^{12}$C	Expt.	0.52 ± 0.02	0.74 ± 0.02	−0.29 ± 0.03	1.26	0.959
Central	QGSM	0.55 ± 0.01	0.77 ± 0.01	−0.32 ± 0.02	1.99	0.980
$d + {}^{12}$C	Expt.	0.178 ± 0.004	0.80 ± 0.01	0.03 ± 0.02	0.86	0.986
Peripheral	QGSM	0.176 ± 0.003	0.80 ± 0.01	−0.10 ± 0.01	2.79	0.985
^{12}C + ^{12}C	Expt.	1.44 ± 0.02	0.774 ± 0.006	−0.021 ± 0.009	2.52	0.990
Central	QGSM	1.63 ± 0.02	0.794 ± 0.006	0.009 ± 0.009	2.97	0.989
^{12}C + ^{12}C	Expt.	0.274 ± 0.003	0.813 ± 0.006	−0.008 ± 0.009	2.76	0.991
Peripheral	QGSM	0.289 ± 0.004	0.797 ± 0.006	−0.006 ± 0.009	7.32	0.972
^{12}C + ^{181}Ta	Expt.	3.10 ± 0.07	0.68 ± 0.01	−0.52 ± 0.01	3.63	0.958
Central	QGSM	4.02 ± 0.09	0.66 ± 0.01	−0.48 ± 0.01	21.06	0.837
^{12}C + ^{181}Ta	Expt.	0.59 ± 0.01	0.81 ± 0.01	−0.08 ± 0.02	2.82	0.967
Peripheral	QGSM	0.70 ± 0.01	0.78 ± 0.01	−0.09 ± 0.02	7.19	0.937

TABLE V. The widths of the rapidity spectra of the negative pions and charged kaons in central Pb + Pb collisions at 20A and 30A GeV extracted from fitting with the Gaussian function by the NA49 Collaboration in Ref. [39].

Type	Central Pb + Pb collisions	
	20A GeV	30A GeV
π^-	0.837 ± 0.007	0.885 ± 0.007
K^+	0.601 ± 0.012	0.722 ± 0.026
K^-	0.642 ± 0.035	0.710 ± 0.032

worth mentioning. The rapidity distributions of the participant protons in these collisions changed drastically with an increase in collision centrality. The QGSM could describe the change in shape of the rapidity spectra of the participant protons with increasing centrality in the above collisions quite well. Two distinct peaks, which correspond to target and projectile protons, were observed for the rapidity spectra of the participant protons in peripheral ^{12}C + ^{12}C and ^{12}C + ^{181}Ta collisions. With increasing collision centrality, the projectile and target peaks overlapped, and a central plateau developed in central ^{12}C + ^{12}C collisions. It was shown [22] that an increase in the number of protons from resonance decays, which mainly occupy the central rapidity region, led to the appearance of plateau in central ^{12}C + ^{12}C collisions. In ^{12}C + ^{181}Ta collisions, the target peak was more prominent in peripheral collisions as compared to peripheral ^{12}C + ^{12}C collisions due to projectile-target asymmetry. However, in central ^{12}C + ^{181}Ta collisions, only a steep asymmetric peak appeared due to the almost complete projectile stopping by the target nuclei [37]. The rapidity distributions for the $Z = 1$ particles also showed strong centrality dependence in Ca + Ca, N + N, Ne + Au, and Au + Au collisions at the energy range from 250 to 2100 MeV per nucleon in Ref. [40]. Similarly, the strong centrality dependence for the rapidity spectra of the protons in Si + Al and Au + Au collisions at 14.6 and 11.6 GeV/c per nucleon was observed in Refs. [41,42].

The observed differences between the rapidity spectra of the negative pions and the participant protons are likely due to large differences in the threshold energies required for the production of such particles. Since protons are readily available in the colliding nuclei, the excitation energies of the order of 10 MeV/nucleon are sufficient for the emission of protons from the nuclei. Therefore, protons are produced easily during the fragmentation of the colliding nuclei in peripheral collisions, which results in the appearance of two distinct peaks in their rapidity spectra that correspond to target and projectile fragmentation regions. On the other hand, pions are not readily present in the colliding nuclei, and the threshold energy for their production is about 300 MeV. Hence, the dominant fraction of pions is produced at the midrapidity region around the center-of-mass rapidity of the participant nucleons both in peripheral and in central nucleus-nucleus collisions. This can explain the single peak structure of the rapidity distributions of the negative pions observed in both central and peripheral d + ^{12}C, ^{12}C + ^{12}C, and ^{12}C + ^{181}Ta collisions at 4.2A GeV/c.

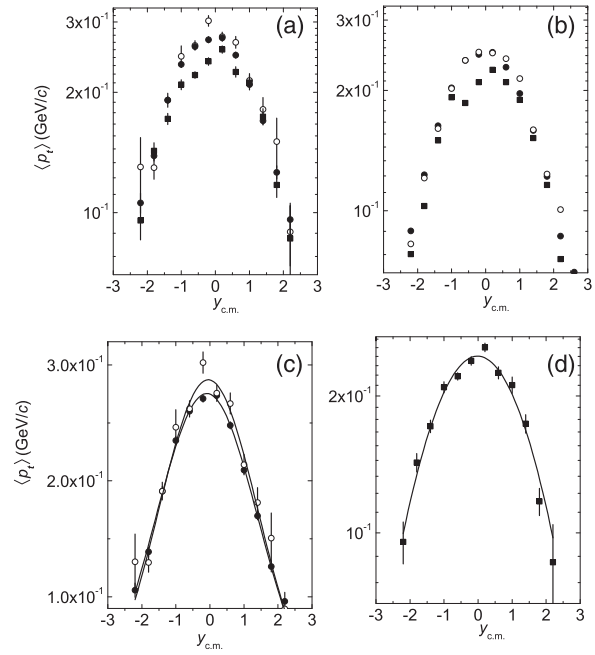

FIG. 4. (a) The experimental $\langle p_t \rangle$ versus $y_{c.m.}$ spectra of the negative pions in d + ^{12}C (○), ^{12}C + ^{12}C (●), and ^{12}C + ^{181}Ta (■) collisions at 4.2A GeV/c; (b) the same as in (a) for the QGSM spectra; (c) the experimental $\langle p_t \rangle$ versus $y_{c.m.}$ spectra of the negative pions in d + ^{12}C (○) and ^{12}C + ^{12}C (●) collisions at 4.2A GeV/c along with the corresponding fits (solid lines) with the Gaussian function; and (d) the experimental $\langle p_t \rangle$ versus $y_{c.m.}$ spectra of the negative pions in ^{12}C + ^{181}Ta (■) collisions at 4.2A GeV/c along with the corresponding fit (solid line) with the Gaussian function. All the spectra are obtained in the c.m.s. of the nucleon-nucleon collisions at 4.2 GeV/c.

Figure 4(a) shows the comparison of dependences of the experimental mean-transverse momenta of the negative pions on their nucleon-nucleon c.m.s. rapidities in d + ^{12}C, ^{12}C + ^{12}C, and ^{12}C + ^{181}Ta collisions at 4.2 GeV/c per nucleon. It is obvious from Fig. 4(a) that high p_t π^- mesons are produced in the central rapidity region, whereas, the projectile and target fragmentation regions are occupied by the low-p_t negative pions. It can be seen from Fig. 4(a) that the height of the peak of $\langle p_t \rangle$ versus the rapidity spectrum decreases with an increase in projectile or target nucleus mass. As evident from Fig. 4(a), the values of the mean-transverse momenta of the π^- mesons are smaller around the target fragmentation region $y_{c.m.} < 0$ in ^{12}C + ^{181}Ta collisions as compared to d + ^{12}C and ^{12}C + ^{12}C collisions. This is obviously due to the reason that, in the case of ^{12}C + ^{181}Ta collisions, the projectile nucleons have to undergo more collisions (interactions) with more nucleons of a heavy ^{181}Ta target as compared to d + ^{12}C and ^{12}C + ^{12}C collisions at the same incident momentum per nucleon. Therefore, the energy transferred during collision is shared among the greater number of participant nucleons (and, hence, the larger number of produced pions) in ^{12}C + ^{181}Ta collisions as compared to d + ^{12}C and ^{12}C + ^{12}C collisions. This causes, as seen from Fig. 4(a), the visible deviation from the Gaussian bell-like shape of $\langle p_t \rangle$ versus the rapidity spectrum of the negative pions in ^{12}C + ^{181}Ta collisions as compared to d + ^{12}C and ^{12}C + ^{12}C collisions.

TABLE VI. Parameters extracted from fitting the $\langle p_t \rangle$ versus $y_{\text{c.m.}}$ spectra of the negative pions in $d + {}^{12}\text{C}$, ${}^{12}\text{C} + {}^{12}\text{C}$, and ${}^{12}\text{C} + {}^{181}\text{Ta}$ collisions at 4.2 GeV/c per nucleon with the Gaussian function.

	Type	A_0 (GeV/c)	σ	y_0	χ^2/n.d.f.	R^2 value
$d + {}^{12}\text{C}$	Expt.	0.42 ± 0.01	1.46 ± 0.04	−0.05 ± 0.03	1.32	0.972
	QGSM	0.381 ± 0.005	1.50 ± 0.02	0.03 ± 0.02	1.29	0.993
${}^{12}\text{C} + {}^{12}\text{C}$	Expt.	0.416 ± 0.004	1.51 ± 0.02	−0.09 ± 0.01	1.05	0.996
	QGSM	0.376 ± 0.003	1.50 ± 0.02	−0.03 ± 0.01	0.79	0.998
${}^{12}\text{C} + {}^{181}\text{Ta}$	Exper	0.40 ± 0.01	1.63 ± 0.04	−0.01 ± 0.03	2.09	0.967
	QGSM	0.354 ± 0.006	1.64 ± 0.03	0.08 ± 0.02	10.63	0.937

Corresponding to Fig. 4(a) dependences, calculated using QGSM, are presented in Fig. 4(b). As can be seen from Fig. 4(b), the model spectra satisfactorily describe the behavior of the corresponding experimental spectra given in Fig. 4(a). Figure 4(b) shows that the height of a peak of the model spectrum as well as the values of $\langle p_t \rangle$ in the target fragmentation region $y_{\text{c.m.}} < 0$ are smaller in the case of ${}^{12}\text{C} + {}^{181}\text{Ta}$ collisions as compared to $d + {}^{12}\text{C}$ and ${}^{12}\text{C} + {}^{12}\text{C}$ collisions. Similar behavior also was observed for the experimental spectra illustrated in Fig. 4(a).

The experimental $\langle p_t \rangle$ versus $y_{\text{c.m.}}$ spectra of the negative pions in $d + {}^{12}\text{C}$, ${}^{12}\text{C} + {}^{12}\text{C}$, and ${}^{12}\text{C} + {}^{181}\text{Ta}$ collisions at 4.2A GeV/c along with the corresponding fits with the Gaussian function are presented in Figs. 4(c) and 4(d). The corresponding parameters extracted from fitting the $\langle p_t \rangle$ versus $y_{\text{c.m.}}$ spectra of the negative pions in $d + {}^{12}\text{C}$, ${}^{12}\text{C} + {}^{12}\text{C}$, and ${}^{12}\text{C} + {}^{181}\text{Ta}$ collisions at 4.2 GeV/c per nucleon with the Gaussian function are presented in Table VI. As can be seen from Figs. 4(c) and 4(d) and the values of χ^2/n.d.f. and R^2 from Table VI, all the $\langle p_t \rangle$ versus $y_{\text{c.m.}}$ spectra, except for the spectrum for ${}^{12}\text{C} + {}^{181}\text{Ta}$ collisions (which somewhat deviates from the Gaussian shape), are fitted quite satisfactorily with the Gaussian function. The values of the extracted widths, as seen from Table VI, are compatible with each other and with the corresponding QGSM results in the analyzed collisions. One can notice that the centers y_0 of $\langle p_t \rangle$ versus $y_{\text{c.m.}}$ spectra of the negative pions in $d + {}^{12}\text{C}$, ${}^{12}\text{C} + {}^{12}\text{C}$, and ${}^{12}\text{C} + {}^{181}\text{Ta}$ collisions are located very close to midrapidity $y_{\text{c.m.}} = 0$ and do not depend on the masses of the target and projectile nuclei.

Furthermore, we studied the dependences of $\langle p_t \rangle$ versus $y_{\text{c.m.}}$ spectra of negative pions in the analyzed collisions on the collision centrality. The experimental $\langle p_t \rangle$ versus $y_{\text{c.m.}}$ spectra of the negative pions in central and peripheral $d + {}^{12}\text{C}$, ${}^{12}\text{C} + {}^{12}\text{C}$, and ${}^{12}\text{C} + {}^{181}\text{Ta}$ collisions at 4.2A GeV/c along with the corresponding fits with the Gaussian function are shown in Fig. 5. The corresponding parameters extracted from fitting the $\langle p_t \rangle$ versus $y_{\text{c.m.}}$ spectra of the negative pions in central and peripheral $d + {}^{12}\text{C}$, ${}^{12}\text{C} + {}^{12}\text{C}$, and ${}^{12}\text{C} + {}^{181}\text{Ta}$ collisions with the Gaussian function in the experiment and the QGSM are displayed in Table VII. As can be seen from Fig. 5, all the spectra are described quite satisfactorily by the Gaussian function. For all the collisions under consideration, as observed from Fig. 5, the corresponding spectra for central and peripheral collisions coincide within uncertainties. As seen from Table VII, the widths extracted for central and peripheral $d + {}^{12}\text{C}$, ${}^{12}\text{C} + {}^{12}\text{C}$, and ${}^{12}\text{C} + {}^{181}\text{Ta}$ collisions are compatible within uncertainties with each other and with the corresponding QGSM results. From Table VII, it is seen that the centers y_0 of the $\langle p_t \rangle$ versus $y_{\text{c.m.}}$ spectra of the negative pions in the analyzed central and peripheral collisions are very close to $y_{\text{c.m.}} = 0$ and do not depend on the collision centrality.

For the sake of comparison, it is interesting to consider the rapidity as well as the $\langle p_t \rangle$ versus $y_{\text{c.m.}}$ spectra of the negative pions in nucleon-nucleon collisions at the same incident momentum per nucleon. For this purpose, we extracted 5023 proton-proton inelastic collision events from the experimental database of collisions of protons at 4.2 GeV/c with C_3H_8 in the 2-m propane bubble chamber of JINR (Dubna, Russia). The experimental rapidity as well as the $\langle p_t \rangle$ versus $y_{\text{c.m.}}$ spectra of the negative pions in proton-proton collisions at 4.2 GeV/c along with the corresponding model spectra and fits with the

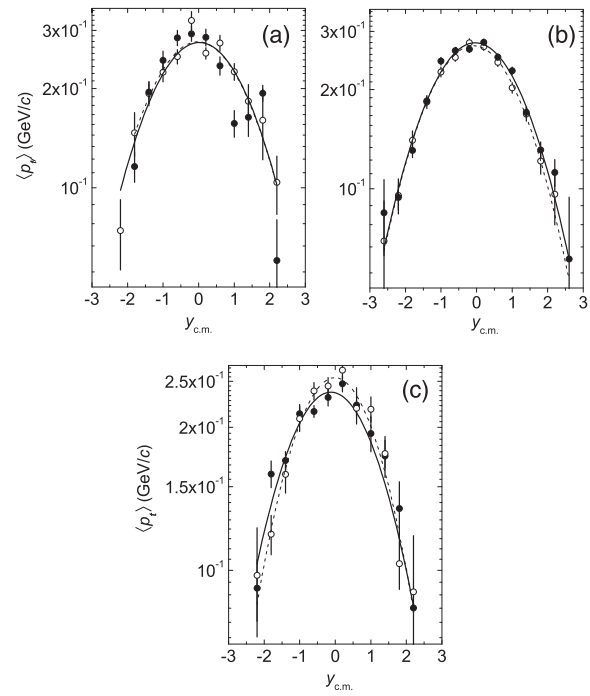

FIG. 5. The experimental $\langle p_t \rangle$ versus $y_{\text{c.m.}}$ spectra of the negative pions in the central (•) and peripheral (○) collision events in (a) $d + {}^{12}\text{C}$, (b) ${}^{12}\text{C} + {}^{12}\text{C}$, and (c) ${}^{12}\text{C} + {}^{181}\text{Ta}$ collisions at 4.2A GeV/c. The corresponding fits with the Gaussian function for the central and peripheral collisions are given by the solid and dashed lines, respectively. All the spectra are obtained in the c.m.s. of the nucleon-nucleon collisions at 4.2 GeV/c.

TABLE VII. Parameters extracted from fitting the $\langle p_t \rangle$ versus $y_{\text{c.m.}}$ spectra of the negative pions in central and peripheral $d + {}^{12}\text{C}$, ${}^{12}\text{C} + {}^{12}\text{C}$, and ${}^{12}\text{C} + {}^{181}\text{Ta}$ collisions at 4.2 GeV/c per nucleon with the Gaussian function.

Type		A_0 (GeV/c)	σ	y_0	χ^2/n.d.f.	R^2 value
$d + {}^{12}\text{C}$	Expt.	0.43 ± 0.01	1.57 ± 0.07	−0.02 ± 0.05	8.02	0.705
Central	QGSM	0.376 ± 0.009	1.46 ± 0.04	−0.02 ± 0.03	1.67	0.970
$d + {}^{12}\text{C}$	Expt.	0.43 ± 0.02	1.54 ± 0.08	0.02 ± 0.06	1.44	0.924
Peripheral	QGSM	0.377 ± 0.006	1.49 ± 0.03	0.04 ± 0.02	0.95	0.991
${}^{12}\text{C} + {}^{12}\text{C}$	Expt.	0.42 ± 0.01	1.52 ± 0.03	−0.03 ± 0.02	2.10	0.980
Central	QGSM	0.382 ± 0.005	1.54 ± 0.03	−0.04 ± 0.02	1.19	0.990
${}^{12}\text{C} + {}^{12}\text{C}$	Expt.	0.40 ± 0.01	1.49 ± 0.04	−0.08 ± 0.03	0.34	0.993
Peripheral	QGSM	0.371 ± 0.005	1.48 ± 0.03	−0.02 ± 0.02	0.97	0.992
${}^{12}\text{C} + {}^{181}\text{Ta}$	Expt.	0.38 ± 0.01	1.61 ± 0.04	−0.12 ± 0.04	1.68	0.987
Central	QGSM	0.34 ± 0.02	1.70 ± 0.08	0.03 ± 0.07	5.97	0.903
${}^{12}\text{C} + {}^{181}\text{Ta}$	Expt.	0.38 ± 0.01	1.48 ± 0.06	−0.01 ± 0.04	1.19	0.955
Peripheral	QGSM	0.371 ± 0.005	1.48 ± 0.03	−0.02 ± 0.02	0.97	0.992

Gaussian function are illustrated in Fig. 6. The corresponding parameters extracted from fitting the experimental rapidity and the $\langle p_t \rangle$ versus $y_{\text{c.m.}}$ spectra of the negative pions in proton-proton collisions at 4.2 GeV/c with the Gaussian function are given in Table VIII. As seen from Fig. 6 and Table VIII, the experimental rapidity distribution as well as the $\langle p_t \rangle$ versus $y_{\text{c.m.}}$ spectrum of the negative pions in proton-proton collisions are fitted well with the Gaussian function. The so-obtained width of the rapidity spectrum of the π^- mesons in proton-proton collisions proved to be compatible within uncertainties with the corresponding widths of the rapidity spectra of π^- in $d + {}^{12}\text{C}$, ${}^{12}\text{C} + {}^{12}\text{C}$, and ${}^{12}\text{C} + {}^{181}\text{Ta}$ collisions, given in Table II. As can be seen from Tables VI and VIII, the width of the $\langle p_t \rangle$ versus $y_{\text{c.m.}}$ spectrum of the negative pions in proton-proton collisions is noticeably smaller than the corresponding widths in $d + {}^{12}\text{C}$, ${}^{12}\text{C} + {}^{12}\text{C}$, and ${}^{12}\text{C} + {}^{181}\text{Ta}$ collisions. The larger width extracted in nucleus-nucleus collisions as compared to proton-proton collisions at the same incident momentum per nucleon could be due to the multiple scattering effects or/and the influence of Fermi motion on the widths obtained in nucleus-nucleus collisions.

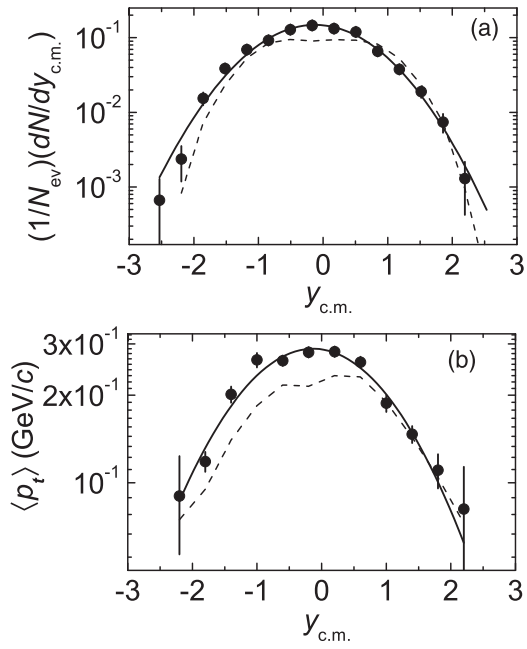

FIG. 6. (a) The experimental rapidity distribution of the negative pions in the proton-proton collisions at 4.2 GeV/c and (b) the experimental $\langle p_t \rangle$ versus $y_{\text{c.m.}}$ spectrum of the negative pions in the proton-proton collisions at 4.2 GeV/c; the model spectra and the fits of the experimental spectra with the Gaussian function are given by the dashed and solid lines, respectively. All the spectra are obtained in the c.m.s. of the nucleon-nucleon collisions at 4.2 GeV/c.

V. SUMMARY AND CONCLUSIONS

The experimental rapidity as well as the $\langle p_t \rangle$ versus $y_{\text{c.m.}}$ spectra of the negative pions in $d + {}^{12}\text{C}$, ${}^{12}\text{C} + {}^{12}\text{C}$, and ${}^{12}\text{C} + {}^{181}\text{Ta}$ collisions at a momentum of 4.2 GeV/c per nucleon were analyzed. The experimental results were compared systematically with the QGSM calculations, which included the rescattering processes of secondary particles, production of resonances, their interactions, and decays. The widths and centers y_0 of the experimental and QGSM rapidities as well as the $\langle p_t \rangle$ versus $y_{\text{c.m.}}$ spectra of the negative pions were extracted from fitting with the Gaussian function. All the rapidities as well as the $\langle p_t \rangle$ versus $y_{\text{c.m.}}$ spectra of the negative pions in the analyzed collisions, except for the $\langle p_t \rangle$ versus $y_{\text{c.m.}}$ spectrum of π^- in the ${}^{12}\text{C} + {}^{181}\text{Ta}$ collisions (which somewhat deviated from the Gaussian shape), possessed Gaussian bell-like shapes and could be fitted quite satisfactorily with the Gaussian function. The centers y_0 of the rapidity distributions of the π^- mesons extracted from fitting with the Gaussian function coincided within uncertainties with the corresponding mean rapidities of the negative pions in the analyzed collisions. This shows that the analyzed rapidity spectra of the negative pions were approximately symmetric around their centers. The widths of the rapidity distributions of the π^- mesons practically coincided in $d + {}^{12}\text{C}$ and ${}^{12}\text{C} + {}^{12}\text{C}$ collisions, whereas, it was slightly smaller in the case of ${}^{12}\text{C} + {}^{181}\text{Ta}$ collisions both in the experiment and in the QGSM.

The widths of the experimental rapidity spectra of the negative pions decreased by (8 ± 2)%, (5 ± 1)%, and (15 ±

TABLE VIII. Parameters extracted from fitting the experimental rapidity and $\langle p_t \rangle$ versus $y_{\text{c.m.}}$ spectra of the negative pions in proton-proton collisions at 4.2 GeV/c with the Gaussian function.

Type	A_0	σ	y_0	χ^2/n.d.f.	R^2 value
Rapidity spectrum	0.117 ± 0.003	0.79 ± 0.01	−0.12 ± 0.02	1.18	0.989
$\langle p_t \rangle$ versus $y_{\text{c.m.}}$ spectrum	0.38 ± 0.01	1.33 ± 0.04	−0.13 ± 0.03	1.38	0.966

2)% in going from peripheral to central $d + {}^{12}\text{C}$, ${}^{12}\text{C} + {}^{12}\text{C}$, and ${}^{12}\text{C} + {}^{181}\text{Ta}$ collisions, respectively. The centers y_0 of the experimental rapidity distributions of the π^- mesons shifted by -0.32 ± 0.04 and -0.44 ± 0.02 units towards the target fragmentation region while going from peripheral to central $d + {}^{12}\text{C}$ and ${}^{12}\text{C} + {}^{181}\text{Ta}$ collisions, respectively. Such shifts in y_0 of the rapidity spectra of the π^- mesons in the case of $d + {}^{12}\text{C}$ and ${}^{12}\text{C} + {}^{181}\text{Ta}$ collisions could be explained by an increase in the rescattering effects in the target nuclei, which are heavier than the projectile nuclei, and the subsequent increase in the numbers of target participant nucleons and pions produced in the target fragmentation region with an increase in collision centrality. On the whole, the degree of shift in y_0 and the decrease in the width of the rapidity spectra of the negative pions in going from peripheral to central collisions correlated with the ratio of mass numbers of the target and projectile nuclei. The absolute values of the shift in y_0 and decrease in a width of the rapidity spectra of the π^- mesons increased as this ratio increased in correspondence with the relation $\frac{A(^{12}\text{C})}{A(^{12}\text{C})} < \frac{A(^{12}\text{C})}{A(^{2}\text{H})} < \frac{A(^{181}\text{Ta})}{A(^{12}\text{C})}$.

The values of the widths of the $\langle p_t \rangle$ versus $y_{\text{c.m.}}$ spectra of the negative pions in $d + {}^{12}\text{C}$, ${}^{12}\text{C} + {}^{12}\text{C}$, and ${}^{12}\text{C} + {}^{181}\text{Ta}$ collisions proved to be compatible with each other and with the corresponding QGSM results. The centers y_0 of the $\langle p_t \rangle$ versus $y_{\text{c.m.}}$ spectra of the negative pions in $d + {}^{12}\text{C}$, ${}^{12}\text{C} + {}^{12}\text{C}$, and ${}^{12}\text{C} + {}^{181}\text{Ta}$ collisions were located very close to midrapidity $y_{\text{c.m.}} = 0$ and did not depend on the masses of the target and projectile nuclei.

The extracted widths of the $\langle p_t \rangle$ versus $y_{\text{c.m.}}$ spectra of the negative pions in central and peripheral $d + {}^{12}\text{C}$, ${}^{12}\text{C} + {}^{12}\text{C}$, and ${}^{12}\text{C} + {}^{181}\text{Ta}$ collisions were compatible within uncertainties with each other and with the corresponding QGSM results and, hence, did not depend on the collision centrality. Similarly, the locations of centers y_0 of the $\langle p_t \rangle$ versus $y_{\text{c.m.}}$ spectra of the negative pions in the analyzed central and peripheral collisions were very close to $y_{\text{c.m.}} = 0$ and did not depend on the collision centrality.

The width of the rapidity spectrum of the π^- mesons extracted for proton-proton collisions at 4.2 GeV/c was compatible within the uncertainties with the corresponding widths of the rapidity spectra of π^- in $d + {}^{12}\text{C}$, ${}^{12}\text{C} + {}^{12}\text{C}$, and ${}^{12}\text{C} + {}^{181}\text{Ta}$ collisions at 4.2 GeV/c per nucleon. The noticeably larger widths of the $\langle p_t \rangle$ versus $y_{\text{c.m.}}$ spectra of the negative pions in $d + {}^{12}\text{C}$, ${}^{12}\text{C} + {}^{12}\text{C}$, and ${}^{12}\text{C} + {}^{181}\text{Ta}$ collisions as compared to the proton-proton collisions could be explained by the multiple scattering effects or/and by the influence of Fermi motion on the widths extracted in the nucleus-nucleus collisions.

On the whole, the QGSM could quite satisfactorily describe the analyzed experimental spectra of the negative pions in $d + {}^{12}\text{C}$, ${}^{12}\text{C} + {}^{12}\text{C}$, and ${}^{12}\text{C} + {}^{181}\text{Ta}$ collisions at 4.2 GeV/c per nucleon.

ACKNOWLEDGMENTS

We are grateful to the staff of the Laboratory of High Energies of JINR (Dubna, Russia) and of the Laboratory of Multiple Processes of Physical-Technical Institute of Uzbek Academy of Sciences (Tashkent, Uzbekistan) for processing the stereophotographs from the 2-m propane bubble chamber of JINR and the significant increase in statistics of the measured nucleus-nucleus collision events at 4.2A GeV/c. Kh. K. O. is thankful to the Higher Education Commission (HEC) of the Government of Pakistan for support under the Foreign Faculty Hiring Program (FFHP). A.I. is grateful for a Ph.D. grant provided by HEC Research Project No. 1925.

[1] D. Krpić, G. Škoro, I. Pićurić, S. Backović, and S. Drndarević, Phys. Rev. C **65**, 034909 (2002).
[2] Kh. K. Olimov, Phys. Rev. C **76**, 055202 (2007).
[3] Kh. K. Olimov, S. L. Lutpullaev, B. S. Yuldashev, Y. H. Huseynaliyev, and A. K. Olimov, Eur. Phys. J. A **44**, 43 (2010).
[4] Kh. K. Olimov, Phys. At. Nucl. **73**, 433 (2010).
[5] Kh. K. Olimov, S. L. Lutpullaev, K. Olimov, K. G. Gulamov, and J. K. Olimov, Phys. Rev. C **75**, 067901 (2007).
[6] Kh. K. Olimov and M. Q. Haseeb, Eur. Phys. J. A **47**, 79 (2011).
[7] Kh. K. Olimov, M. Q. Haseeb, A. K. Olimov, and I. Khan, Cent. Eur. J. Phys. **9**, 1393 (2011).
[8] Kh. K. Olimov, M. Q. Haseeb, I. Khan, A. K. Olimov, and V. V. Glagolev, Phys. Rev. C **85**, 014907 (2012).
[9] Kh. K. Olimov, M. Q. Haseeb, and I. Khan, Phys. At. Nucl. **75**, 479 (2012).
[10] B.-A. Li and W. Bauer, Phys. Rev. C **44**, 450 (1991); B.-A. Li and C. M. Ko, *ibid.* **52**, 2037 (1995).
[11] W. Ehehalt, W. Cassing, A. Engel, U. Mosel, and G. Wolf, Phys. Lett. B **298**, 31 (1993).
[12] M. Eskef *et al.* (FOPI Collaboration), Eur. Phys. J. A **3**, 335 (1998).

[13] J. Barrette *et al.* (E814 Collaboration), Phys. Lett. B **351**, 93 (1995).
[14] G. E. Brown, J. Stachel, and G. M. Welke, Phys. Lett. B **253**, 19 (1991).
[15] R. Brockmann, J. W. Harris, A. Sandoval, R. Stock, H. Ströbele, G. Odyniec, H. G. Pugh, L. S. Schroeder, R. E. Renfordt, D. Schall, D. Bangert, W. Rauch, and K. L. Wolf, Phys. Rev. Lett. **53**, 2012 (1984).
[16] L. Chkhaidze *et al.*, Bull. Georgian Acad. Sci. **4**, 41 (2010).
[17] S. Backović, D. Salihagić, L. Simić, D. Krpić, S. Drndarević, R. R. Mekhdiyev, A. P. Cheplakov, H. N. Agakishiev, E. N. Kladnitskaya, and S. Y. Sivoklokov, Phys. Rev. C **46**, 1501 (1992).
[18] Kh. K. Olimov and M. Q. Haseeb, Phys. At. Nucl. **76**, 595 (2013).
[19] Kh. K. Olimov, M. Q. Haseeb, and S. A. Hadi, Int. J. Mod. Phys. E **22**, 1350020 (2013).
[20] R. Hagedorn and J. Rafelski, Phys. Lett. B **97**, 136 (1980).
[21] R. Hagedorn and J. Ranft, Nuovo Cimento, Suppl. **6**, 169 (1968).
[22] L. Simić, S. Backović, D. Salihagić, A. P. Cheplakov, E. N. Kladnitskaya, and R. R. Mekhdiyev, Phys. Rev. C **52**, 356 (1995).
[23] R. N. Bekmirzaev, E. N. Kladnitskaya, and S. A. Sharipova, Phys. At. Nucl. **58**, 58 (1995).
[24] R. N. Bekmirzaev, E. N. Kladnitskaya, M. M. Muminov, and S. A. Sharipova, Phys. At. Nucl. **58**, 1721 (1995).
[25] L. Chkhaidze, T. Djobava, L. Kharkhelauri, and M. Mosidze, Eur. Phys. J. A **1**, 299 (1998).
[26] V. D. Toneev, N. S. Amelin, K. K. Gudima, and S. Y. Sivoklokov, Nucl. Phys. A **519**, 463c (1990).
[27] N. S. Amelin, K. K. Gudima, S. Y. Sivoklokov, and V. D. Toneev, Sov. J. Nucl. Phys. **52**, 172 (1990).
[28] N. S. Amelin, K. K. Gudima, and V. D. Toneev, Sov. J. Nucl. Phys **51**, 1093 (1990).
[29] N. S. Amelin, E. F. Staubo, L. P. Csernai, V. D. Toneev, and K. K. Gudima, Phys. Rev. C **44**, 1541 (1991).
[30] A. I. Bondarenko *et al.*, Phys. At. Nucl. **65**, 90 (2002).
[31] L. Chkhaidze, T. Djobava, and L. Kharkhelauri, Bull. Georgian Acad. Sci. **6**, 44 (2012).
[32] K. Olimov, S. L. Lutpullaev, A. K. Olimov, V. I. Petrov, and S. A. Sharipova, Phys. At. Nucl. **73**, 1847 (2010).
[33] L. Chkhaidze, P. Danielewicz, T. Djobava, L. Kharkhelauri, and E. Kladnitskaya, Nucl. Phys. A **794**, 115 (2007).
[34] G. N. Agakishiyev *et al.*, Z. Phys. C **27**, 177 (1985).
[35] D. Armutlisky *et al.*, Z. Phys. A **328**, 455 (1987).
[36] A. I. Bondarenko *et al.*, JINR Report No. P1-98-292, 1998 (unpublished).
[37] S. Backovic, V. Boldea, V. G. Grishin, S. Ditza *et al.*, Sov. J. Nucl. Phys. **50**, 1001 (1989).
[38] M. I. Adamovich *et al.* (EMU01 Collaboration), Phys. Rev. Lett. **69**, 745 (1992).
[39] C. Alt *et al.* (NA49 Collaboration), Phys. Rev. C **77**, 024903 (2008).
[40] H. H. Gutbrod *et al.*, Z. Phys. A **337**, 57 (1990).
[41] M. Gonin *et al.*, Nucl. Phys. A **566**, 601c (1994).
[42] J. Stachel *et al.*, Nucl. Phys. A **566**, 183c (1994).